

# A Model for WLAN Signal Attenuation of the Human Body

Ngewi Fet  
University of Duisburg-Essen,  
Germany  
ngewi.fet@uni-due.de

Marcus Handte  
University of Duisburg-Essen,  
Germany  
marcus.handte@uni-due.de

Pedro José Marrón  
University of Duisburg-Essen,  
Germany  
pjmarron@uni-due.de

## ABSTRACT

Fingerprinting-based indoor localization involves building a signal strength radio map. This map is usually built manually by a person holding the mapping device, which results in orientation-dependent fingerprints due to signal attenuation by the human body. To offset this distortion, fingerprints are typically collected for multiple orientations, but this requires a high effort for large localization areas. In this paper, we propose an approach to reduce the mapping effort by modeling the WLAN signal attenuation caused by the human body. By applying the model to the captured signal to compensate for the attenuation, it is possible to generate an orientation-independent fingerprint. We demonstrate that our model is location and person independent and its output is comparable with manually created radio maps. By using the model, the WLAN scanning effort can be reduced by 75% to 87.5% (depending on the number of orientations).

## Author Keywords

Indoor Localization; Signal Attenuation; Signal Modeling

## ACM Classification Keywords

I.6 Simulation and Modeling: Model Development—*Model Validation and Analysis*

## INTRODUCTION

Many WLAN-based indoor localization [1] [6] systems rely on the characteristic received signal strength indicator (RSSI) of the propagated signal throughout a building to estimate a location. For fingerprint-based systems, deployment usually consists of a training phase and a localization phase. A fingerprint of a location in a building comprises the list of visible access points at that location and their corresponding signal strengths. During the training phase, fingerprints are collected by a person - the trainer - at multiple locations across the building and assigned unique coordinates corresponding to the location where the fingerprint was created. This collection of fingerprints is known as the training radio map. In the localization phase, a scan is again performed to capture a fingerprint which is then compared to the fingerprints in the training radio map to find the closest match. The corresponding location coordinates for the matching fingerprint are then retrieved as the estimated location.

WLAN signals are predominantly transmitted in the 2.4 GHz frequency band, which is also the resonance frequency of water [13]. The human body is made of up to 72% water [19], therefore the WLAN signals are significantly absorbed by the trainer during the training phase. This absorption consequently distorts the received signal strength for the access points in the radio map [15]. Considering only one measurement per location results in a radio map where the RSSI measurements are skewed in one orientation due to the presence of the trainer. The error thus introduced by the trainer is systematic and leads to a general degradation in localization performance due to the fact that the users of the system may face any arbitrary orientation during the localization phase.

One of the earliest WLAN-based indoor localization systems employing WLAN fingerprinting was RADAR [1]. To counter the effects of the attenuation, the authors collected training fingerprints in multiple orientations for each location. This helped to build a more orientation-independent fingerprint by collecting the RSSI values for multiple orientations and combining them to take the signal attenuation by the body into account. Through this technique, they achieve localization accuracy improvements of up to 67% (in the worst case). As a result, other systems, e.g. [8], have followed this approach.

Unfortunately, creating multiple fingerprints per location significantly increases the training effort. Especially for large areas, like conference venues or storage facilities, the resulting increase in training effort can be prohibitively high. To avoid this, we propose a signal attenuation model which is able to generate the fingerprints for multiple orientations given the fingerprint for just one orientation, while compensating for signal attenuation due to the human body. With this model, it is possible to reduce the WLAN scanning time for creating a multiple-orientation radio map by up to 75% to 87.5% (depending on the number of orientations), while maintaining overall signal quality characteristics of the localization area and accounting for signal attenuation due to the human body. We demonstrate that our model is location and person independent and can be used to improve localization performance in deployed systems with minimal effort.

The remainder of this paper is structured as follows. The next section discusses related work in the area of indoor localization and WLAN signal propagation modeling. Thereafter, we propose our approach to modeling the signal attenuation caused by the human body. Then in the subsequent sections, we experimentally evaluate the signal attenuation model and finally conclude the paper with a summary and directions for future research.

Permission to make digital or hard copies of all or part of this work for personal or classroom use is granted without fee provided that copies are not made or distributed for profit or commercial advantage and that copies bear this notice and the full citation on the first page. Copyrights for components of this work owned by others than the author(s) must be honored. Abstracting with credit is permitted. To copy otherwise, or to publish, to post on servers or to redistribute to lists, requires prior specific permission and/or a fee. Request permissions from [permissions@acm.org](mailto:permissions@acm.org).

*UbiComp '13*, September 8–12, 2013, Zurich, Switzerland.

Copyright is held by the owner/author(s). Publication rights licensed to ACM.

ACM 978-1-4503-1770-2/13/09...\$15.00.

<http://dx.doi.org/10.1145/2493432.2493459>

## RELATED WORK

Several WLAN-based indoor localization systems have been developed in recent years, and these systems can be broadly categorized into either fingerprinting-based systems or systems which rely on signal propagation modeling for location estimation. The model-based systems typically seek to reduce the effort for creating the training radio map.

Systems which rely on signal propagation modeling do not require a training phase involving manually creating a radio map, and therefore require less on-site effort to set up. Seidel et al [21] present a model for the path loss at 914 MHz and other articles [20] have shown that WLAN signals follow a similar log-normal distribution [3]. Consequently, several localization systems [16] [17] have been built based on WLAN signal propagation models. The propagation of WLAN signals indoors is difficult to model accurately due to the dense multi-path effects in the environment as well as reflection, diffraction and scattering of the signal [13]. The high number of variables involved in signal propagation modeling in indoor environments results in a high modeling effort or limitation of the model variables which can reduce the precision of the model. Many propagation models seek to capture the attenuation and distribution of a signal over distance in an area, whereas our approach focuses on the attenuation caused by the human body at any given position.

Besides model-based systems, there are several systems using WLAN fingerprinting for indoor localization [1] [26] [4] [12]. In RADAR [1] the authors build a signal fingerprint radio map which is used for training and localization. Their findings show that effects of user orientation can cause significant degradation in localization performance. To remedy this, they collect fingerprints for 4 orientations and show that they thus achieve up to 67% improvement in localization accuracy (in the worst case). They also demonstrate that fingerprint-based localization methods provide better performance than signal propagation model based methods. However, the fingerprint-based methods usually have higher deployment effort and training costs. COMPASS [14] is another system that tries to mitigate the effects of the user orientation by using a digital compass to select only the training fingerprints for the user's orientation during localization. They collect several measurements per location for multiple orientations which indicates a high time and effort investment for mapping large areas. SpinLoc [22] requires users to spin around in order to capture a more characteristic fingerprint during localization and improve accuracy. This places the burden of compensating for the signal attenuation on the end-user of the system and might be cumbersome. To reduce the mapping effort, ARIADNE [9] uses a floor construction plan and only a single measurement to dynamically generate the radio map while the system is being used. Other systems such as ARIEL [10] and Calibree [23] as well as simultaneous localization and mapping (SLAM) systems [5] [2] reduce the mapping effort by collecting very little data during deployment and progressively improving the radio map as the users use the system. The downside to this approach is that the localization performance immediately after deployment of the system is poor and only increases with time and more users.

Surveys [6] [18] of localization systems indicate that WLAN fingerprinting-based systems generally achieve high localization accuracy. Our approach seeks to maintain or improve the performance of fingerprint-based WLAN localization while simultaneously reducing, but not completely eliminating, the effort for training the localization system.

## APPROACH

In this section, we present our approach to building the signal attenuation model starting with an analysis of the signal strength distribution around a human body and then proceeding onto the construction of the model based on the results.

### RSSI Distribution Analysis

In RADAR [1], the authors noticed that the WLAN RSSI at any position varied depending on the orientation of the person measuring it. During experiments with localization we observe the same effect, that depending on the orientation of the trainer with respect to the access point, there are significant variations in the RSSI values measured. This effect is consistent irrespective of the device used, the access point or location where the radio map was being created. Kaemarungsi et al [11] demonstrate that the attenuation on the signal due to the human body is stronger when closer to the signal source (in this case, the access point) than when further away from it. We observe a similar pattern in our data and set out to better understand the effect by systematically measuring the RSSI at varying distances and orientations from an access point. We collect a series of fingerprints using a mobile phone with increasing distance from the access point in 1 meter increments, up to 10 meters from the access point. The mobile device was consistently held in front of the trainer for all the measurements since the maximum body area is in the path of the signal and mobile devices are typically held in this position during use. At each position, we measure the RSSI in multiple orientations (8 in total) starting with the 0° orientation facing the access point and progressing in 45° increments. 5 scans are performed per orientation in order to get a stable characteristic signal due to normal fluctuations in the RSSI value. The measurements for each orientation are aggregated using the median function and plotted in a radar chart. Figure 1 shows samples of the results of obtained from the data collected.

As expected, we observe that the signal strength in the direction of the access point is strongest when closest to the access point. Correspondingly, the signal attenuation due to the human body is also strongest when closest to the access point but facing away from it. The highest drop in RSSI is observed at 1m, going from -20 dBm when facing the access point to about -62 dBm when facing the opposite direction to the access point. This is a drop of over 40 dBm, as opposed to the drop of only about 5 dBm when at 10m distance from the access point. With increasing distance from the access point, the level of attenuation also reduces progressively. This is consistent with results obtained in [11] which shows greater skewing of RSSI distributions for stronger signals. We repeated the experiment several times using different access points and mobile devices, as well as with and without obstructions between the access point and mobile device and

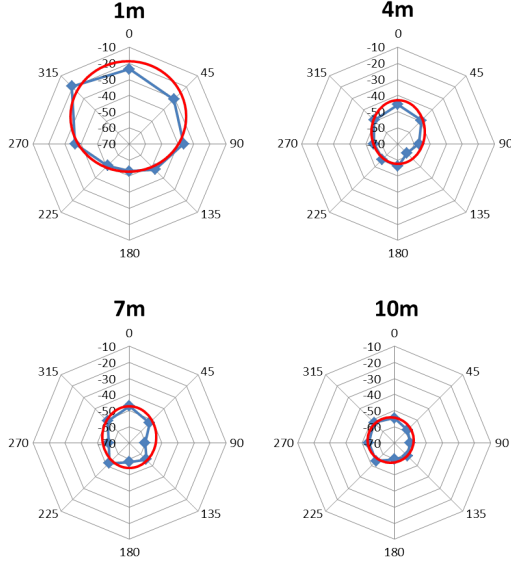


Figure 1. Signal distribution (in dBm) with distance

obtained consistent results. We also performed the same experiment with the access point being at a diagonal from the person and not in a straight line. We noticed that when we rotated our orientations such that the one facing the access point was at  $0^\circ$ , the same pattern emerged. Looking at the distribution of the signal strength around the trainer, we could deduce that the RSSI distribution pattern was circular for weak values and that expanded into an oval shape for strong values. By examining the proportions of the RSSI values when the trainer is facing towards or away from the access point, we conclude that the distribution of the signal strength around the trainer can be approximated with a degenerating elliptical regression with the trainer at one focus of the ellipse. The elliptical regression starts closest to the access point and degenerates into a circular regression with increasing distance. An overlay of the regression on the RSSI values is depicted in Figure 1. Based on these observations, we proceed to model the signal strength distribution around a person based on a degenerating elliptical regression pattern.

### Signal Attenuation Modeling

In the following, we express the degenerating elliptical regression pattern using mathematical statements.

We begin by introducing the basic properties of an ellipse which is a closed loop curve that is symmetric about its horizontal and vertical axes. The parametric equation of an ellipse with respect to the focal point at the origin is given as:

$$r(\theta) = \frac{a * (1 - \epsilon)}{1 - \epsilon * \cos(\theta)} \quad (1)$$

where  $\epsilon$  is the eccentricity of the ellipse,  $\epsilon = \sqrt{1 - \frac{b^2}{a^2}}$ . The variables  $a$  and  $b$  are the semi-major and semi-minor axes of the ellipse respectively as shown in Figure 2 which depicts the basic properties and proportions of an ellipse. The ellipse has two foci  $f_1$  and  $f_2$  which are equidistant (with distance

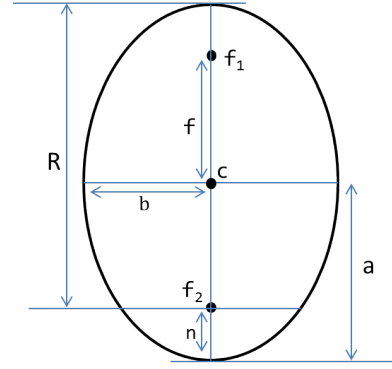


Figure 2. Properties of an ellipse

$f$ ) from the center of the ellipse. If we transpose the ellipse to signal space considering that the trainer is standing at one focus of the ellipse, then the distance in signal space from the focus to the circumference is the RSSI for that given orientation. As we move further away from the access point, the foci move towards the center, eventually merging with it to form a circle.  $R$ , the RSSI when facing the access point depicted in Figure 2 is therefore the maximum RSSI (all other factors being equal) which can be received for that particular access point at a particular location. The RSSI for the different orientations correspond to the distance from the focus  $f_2$  to the different points along the circumference of the ellipse, with the minimum value for the RSSI,  $n$ , occurring when facing opposite the signal source.

Given the parametric equation of the ellipse, we can find the RSSI,  $r(\theta)$  for any given orientation  $\theta$ . However, we need to determine the values for the semi-major and semi-minor axes,  $a$  and  $b$  respectively, which describe the ellipse. Since we have one measurement,  $R$  in the ellipse, we need to express values for  $a$  and  $b$  in terms of this known quantity. From the Figure 2, we can express  $a$  using the following equation:

$$a = \frac{1}{2} * (R + n) \quad (2)$$

In order to express  $n$  in terms of the known quantity  $R$ , we need empirically determine the relationship between the two variables  $R$  and  $n$ .

### Empirical Determination of Coefficients

The mathematical expression of the relationship between the RSSI,  $R$  when facing the access point and the RSSI,  $n$  when facing the opposite direction to the access point is required in order to properly describe the signal distribution due to attenuation in terms of an elliptic regression. Our observations (c.f. Figure 1) indicate that the value of  $n$  varies for different values of  $R$ . To experimentally determine the relationship between  $R$  and  $n$ , we carried out the following experiment.

In our lab, we used 8 access points and placed them equidistant from each other along the circumference of a circle of radius 3m. We then collected fingerprints for 8 different orientations in  $45^\circ$  steps at 9 positions in a  $3 \times 3$  grid within the circle. For each orientation, we scan 5 fingerprints with the mobile device held in front of the trainer and then take then

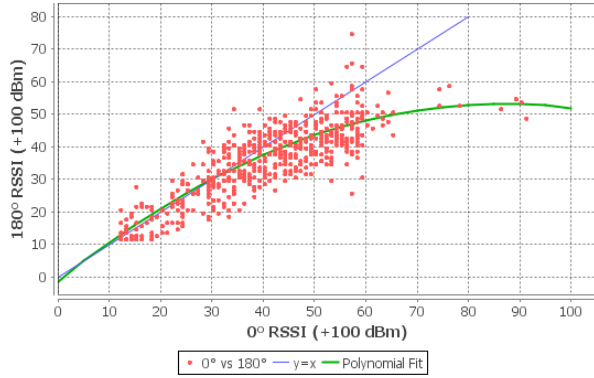


Figure 3. RSSI variations with respect to strongest RSSI

median of the RSSI in order to get a stable fingerprint reading. The arrangement of the access points in a circle guarantees that each time we move to or away from one access point, we correspondingly move away or to another access point. This setup speeds up the collection of data and ensures that we have an equal number of measures both facing and in the opposite direction of each access point for different RSSI values.

We then repeated the experiment with circles of radius 5m, 7m and a partial circle of radius 18m in order to get broad range of signal strength values ranging from very strong to very weak signals. The position and size of the location grid was also adjusted to suit each of the different experiments. After collecting the data, we extracted the signal strengths for each access point across all locations for both the  $0^\circ$  and  $180^\circ$  angles with respect to the access point position. To achieve this, we rotated the orientations in such a way that the orientation in which the trainer was facing the given access point was considered  $0^\circ$  and the orientation where the trainer faces away from the access point was considered  $180^\circ$ . For each location, a different orientation has to be considered as the  $0^\circ$  and  $180^\circ$  measurements with respect to the position of the access point under consideration. By repeating this process for all the access points along the circumference of the circle, it is possible to obtain for each access point the RSSI values both facing it and facing away from it for all locations in the grid.

After extracting all the RSSI values for  $0^\circ$  and  $180^\circ$  per access point, we plot a graph in order to observe how strongly the RSSI  $r(180^\circ)$  is attenuated for different values of RSSI at  $r(0^\circ)$ . At this point, we need to convert the values for the RSSI into positive values in the first quadrant of the Cartesian plane by adding a constant, 100. Using the negative values for RSSI would result in inaccurate representations of the ellipse due to the inversion of the magnitude of the absolute values of  $a$  and  $b$  when the signs canceled out. The resulting graph and the corresponding best fit regression for the data points are shown in Figure 3. It can be observed that the higher the  $r(0^\circ)$  RSSI value, the stronger the attenuation of the  $r(180^\circ)$  value. It can be seen that from RSSI values of -70 dBm or lower in the direction facing the access point, the signal attenuation in the opposite direction is insignificant, resulting

in an almost linear fit. This is due to the fact that the dispersal of the signal at such distances from the access point is already so great that the presence of the human body does not influence the RSSI significantly. The ellipse is therefore degenerated into a circle for all values of  $R < -70dBm$ .

By applying different polynomial regressions to the data taking the best fit, we determine that the relationship between  $R$  and  $n$  matches a quadratic regression which can be generally expressed as

$$n = p * R^2 + q * R + s \quad (3)$$

From the data, we can obtain the equation for the best fit quadratic regression as:

$$y = -0.007316 * x^2 + 1.261967 * x - 1.363591 \quad (4)$$

The coefficients of the quadratic relationship between  $R$  and  $n$  can now be determined as:

$$p = -0.007316, q = 1.261967, s = -1.363591$$

Having determined the coefficients of the quadratic relationship between the RSSI value at  $0^\circ$  ( $R$ ) and the one at  $180^\circ$  ( $n$ ), we can now apply that relationship to the ellipse properties to express the equations for  $a$  and  $b$  solely in terms of  $R$ . By substituting the value for  $n$  in Equation 2, we can express  $a$  solely in terms of  $R$  as follows:

$$a = \frac{1}{2} * (p * R^2 + (1 + q) * R + s) \quad (5)$$

Similarly, we can express the semi-minor axis  $b$  in terms of  $R$  and  $a$  (which is now likewise expressed in terms of  $R$ ). The focus of an ellipse is described by

$$f^2 = a^2 - b^2 \Rightarrow b^2 = a^2 - f^2 \quad (6)$$

However, from Figure 2 it can be seen that

$$f = R - a \quad (7)$$

If we substitute Equation 7 in Equation 6, we get

$$b = \sqrt{a^2 - (R - a)^2} \quad (8)$$

Given the expressions for  $a$  and  $b$  in terms of  $R$ , we can use the parametric equation of an ellipse (Equation 1) to generate the signal strength values for any orientation at a given location. Next, we discuss the process for using the model to enhance a radio map.

### Multiple Signal Sources

Kaemarungsi et al in [13] demonstrate that the RSSI from multiple access points are independent of each other and exhibit the same statistical properties. Consequently, the model developed for one signal source can be extended to multiple signal sources (access points). At any given location, there are multiple signals arriving from different sources with different angles of incidence. However, the trainer only faces a single orientation when performing the scan meanwhile the access points may be situated at very different locations. This implies that we will not be able to observe  $R$  - the strongest signal possible for each access point visible at that location - since we cannot directly face all access points at the same time.

| $R = 0^\circ$ | $45^\circ$ | $90^\circ$ | $135^\circ$ | $180^\circ$ | $225^\circ$ | $270^\circ$ | $315^\circ$ |
|---------------|------------|------------|-------------|-------------|-------------|-------------|-------------|
| -30           | -34        | -41        | -47         | -49         | -47         | -41         | -34         |
| -40           | -43        | -48        | -51         | -53         | -51         | -48         | -43         |
| -50           | -52        | -54        | -56         | -57         | -56         | -54         | -52         |
| -60           | -61        | -62        | -63         | -63         | -63         | -62         | -61         |
| -70           | -70        | -70        | -70         | -70         | -70         | -70         | -70         |

Table 1. Excerpt of the Ellipse Lookup Table (in dBm)

However, to generate the signal strengths for all orientations, we need the value of  $R = r(0^\circ)$  for every access point. We can refactor the parametric equation of the ellipse (Equation 1) in terms of  $a$  and  $b$ , and again in terms of  $R$  (since we have already expressed  $a$  and  $b$  in terms of  $R$ ). The resulting equation enables us to compute the value for  $R$  for any given  $r(\theta)$  and  $\theta$ . Yet, solving the equation for  $R$  results in a multi-page equation with complex numbers which is difficult to work with. Instead, we pre-compute the possible values for  $a$  and  $b$  of the ellipses which describe all possible signal distribution patterns given different values of  $R = r(0^\circ)$ . This is easy since for all practical purposes, the values for  $R$  occur in  $R \in \{0, \dots, -99\}$ , which is a small finite set.

The data set of all possible values for  $a$  and  $b$  is used as a lookup-table for generating the RSSI for different orientations. Given any known RSSI value and the orientation at which it was received as an input tuple  $\{r(\theta), \theta\}$ , we can find the ellipse in the look-up table containing the point  $\{r(\theta), \theta\}$  and retrieve the corresponding  $a$  and  $b$  values of the ellipse. The matching ellipse is then used to compute the RSSI values for all other orientations. Table 1 shows an excerpt of the look-up table, with the generated values for 8 orientations for different values of  $R = r(0^\circ)$ .

### Application to Localization System Deployments

We now have all the parts of the model required for enhancing any single-orientation radio map into one with multiple rotations to improve localization performance. We first consider the case of applying the model to new deployments of indoor localization systems and then follow up with treatment of existing deployments.

#### New Localization System Deployments

When considering the deployment of an indoor localization where the model is to be applied, the required inputs are:

- A radio map with fingerprints of the form

$$V = (X, Y, \theta, \{RSS(AP_1), \dots, RSS(AP_N)\})$$

$\theta$  is the orientation in which trainer was facing when the radio map was built. This can be gotten from a compass or manually recorded when creating the fingerprints.

- Locations  $(X_{ap}, Y_{ap})$  of the access points in the area

Assuming that the access point is located at  $\theta = 0^\circ$  for the measurement in the Cartesian plane, we can use the values for  $\theta$  and  $RSS(AP_i)$  for each access point to look-up the corresponding ellipse (from the pre-computed ellipse data set) describing the signal distribution for that particular location.

However, the orientation at which the fingerprint was captured is not necessarily the same as the orientation with respect to each access point. This is due to the fact that the semi-major axis of each ellipse is considered to be facing the direction  $\theta = 0^\circ$  for each access point. Hence, each access point visible at a location can be considered to be within its own virtual plane which is rotated by a given angle  $\phi$  from the Cartesian plane considered for measurements. Thus, we transpose the angle  $\theta$  from the measurement Cartesian plane to its angle in the signal space plane for each access point.

This is achieved by computing the angle  $\phi$  between the vertical vectors through the fingerprint location  $(X_i, Y_i)$  and the access point location  $(X_{ap}, Y_{ap})$  using Cartesian geometry. This gives us the plane offset between the measurement Cartesian plane and the signal space plane with respect to the access point under consideration at that location. Using this offset, we can then transpose the angle  $\theta$  into the corresponding angle  $\theta_{AP}$  using the formula:

$$\theta_{AP} = ((360 - \phi) + \theta) \quad (9)$$

Now we can look-up the signal distribution ellipse which has a point matching  $\{\theta_{AP}, r(\theta_{AP})\}$ . If no exact match is found, we take the ellipse with the closest RSSI match for  $r(\theta_{AP})$  at  $\theta_{AP}$ . The ellipse is then used to populate the RSSI values for the different orientations at the location. Any variable number of orientations can be computed, although at least 4 orientations is recommended [14]. This is repeated for all access points  $AP_i$  in the fingerprint and in turn for all fingerprints  $V_i$  in the radio map to yield an enhanced radio map which has fingerprints for multiple orientations per fingerprint. The output is a radio map with multiple orientations per location considering the trainer's signal attenuation.

#### Existing Localization System Deployments

The previously described process for applying the model works well when we know where all the access points are and the creation of the initial training radio map is under our control. However, in existing localization system deployments, it may not be known where all access points are deployed, or there may be more visible access points in the location area than are setup, for example signals from other nearby buildings. In such a scenario, we lack an important input required to apply the model to a radio map.

However, the lack of knowledge about the access points' locations can be compensated by dynamically computing them. To do this, we use the approach proposed by Han et al [7] for determining the locations of the access points given a fingerprint radio map. For each access point, we go through all the fingerprints in the radio map where the access point was visible and select the top 2 locations with the highest RSSI for the particular access point. We then take the average of the two locations as the location of the access point.

This simple process enables us to apply the model to the system as previously described. Being able to compute the location of the access points reduces the required inputs for the algorithm to just the radio map. It is thus easy to apply the signal attenuation model to already deployed indoor localization systems.

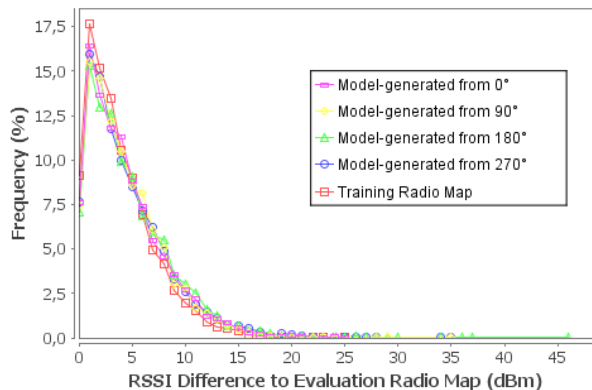


Figure 4. RSSI Deviation for Office Building

| Generated from          | 0°    | 90°   | 180°  | 270°  |
|-------------------------|-------|-------|-------|-------|
| Correlation Coefficient | 0.927 | 0.925 | 0.927 | 0.923 |

Table 2. Correlation of model-generated RSSI to Measured RSSI

## EVALUATION

In this section, we evaluate the performance of the model in terms of its precision with respect to measured fingerprint radio maps, as well as the general applicability of the model to different environments. Furthermore, we compare the localization performance of the model-generated radio maps with manually measured radio maps and single-orientation radio maps. Finally, we discuss how much of a reduction in effort can be achieved by using the model.

### Precision

To evaluate the precision of the model-generated RSSI values, we compute the difference in the RSSI between the measured radio map and the generated radio map and then analyze the distribution of the differences. The following describes in detail how this is done.

We use an Android Galaxy Nexus device to create two radio maps for our office building on two different days, which we label the training and evaluation radio maps respectively. We use only one type of device in this evaluation to eliminate effects of differences in device radios and focus solely on the attenuation caused by the human body. We placed 9 access points at known locations throughout the building. The building has dimensions of 36x15m and we collected fingerprints at 90 locations within the building. At each location, we collected fingerprints for 8 orientations starting from 0° in 45° increments. Then, for each of the orientations in the set {0°, 90°, 180°, 270°}, we remove all other orientations except that one, resulting four single-orientation radio maps (one for each of the 4 orientations). The signal attenuation model is then applied to each of the single-orientation radio maps to generate fingerprints for all other orientations. The differences between each signal in the generated radio map and the original measured radio map are then computed to give the signal variation distribution across all locations.

The RSSI values for WLAN signals at any location are not constant, but vary slightly over consecutive measurements.

Therefore in order to qualify the results of the generated radio map, we also compute the differences between two manually measured training and evaluation radio maps. We compute the deviation in RSSI value for each access point per orientation per location. The distribution of the overall deviation for the generated radio maps and the physical radio map in our office building can be seen in Figure 4.

The distribution of the error for two different manually measured radio maps follows the same pattern as that for the radio maps generated using the model. We further quantify the performance of the model by computing the Pearson correlation coefficient between the generated radio maps and the physical radio map, taking into account the RSSI for each access point at each location. Table 2 shows the correlation for the generated radio maps and the physical radio map.

We observe that there is a strong positive correlation between the generated RSSI values and the measured RSSI values (> 0.9). Moreover, the starting orientation for applying the model has no significant impact on the precision of the output. No matter what orientation is used as the base measurement for generating the radio map, the results are comparable. This indicates that for already deployed indoor localization systems, the signal attenuation model should be applicable regardless of the orientation in which the measurements were taken.

We further break down the deviation per location to observe the effects (if any) of positional dependencies in the observed deviations. The deviation between generated and observed RSSI value for each location in the building is aggregated and plotted using a candlestick representation as seen in Figure 5. The plot shows the minimum, 10th percentile, 90th percentile and maximum deviation aggregated for all access points visible at each location.

It can be observed that there is an even distribution of the RSSI deviation per location for the generated radio map. 90% of all the values typically lie within 0 dBm and 9 dBm. This distribution is similar to the one observed between 2 manually created radio maps. There are also a few outliers which go up to 23 dBm, but these are also observable in the difference distribution between two consecutive measurements at the same location in the building. We can conclude from the observations that the model is (at least) applicable to our office environment.

### General Applicability

To validate the independence of the model from other factors such as the localization area and the trainer, we collected fingerprints in 2 other environments and by 2 different persons. This brings the total tested environments (including the office environment) to 3. The other two buildings were our university library building and a home environment. Also, we selected people of different weights - 90kg and 70kg - to evaluate the attenuation for different body masses. Again each of the trainers created two sets of fingerprint radio maps for each building at two different times of the day. In these environments, we do not know where the access points are located and dynamically compute their locations using the ra-

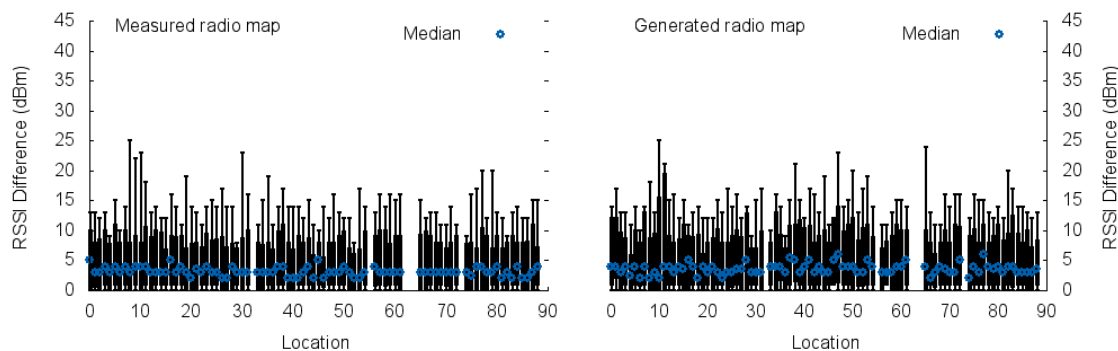


Figure 5. RSSI Deviation per Location for Office Building

radio maps as mentioned previously. The same procedure for evaluating the precision - using the differences between the generated and a measured radio map - was then applied to the data set from each of the environments. The results obtained are illustrated in Figures 6 and 7.

The deviation between the two manually measured maps and the generated maps is comparable. The breakdown of the total deviations per location (Figures 9 and 8) shows that although the maximum deviations for the candlestick values tend to be generally higher, the ranges for the deviations up to the 90th percentile are comparable. The median value for the measured radio maps and the generated radio maps follow the same linear pattern for each of the positions and each of the buildings and averages at 4 dBm. This indicates that the model continues to work for other environments even if we do not know the physical access point locations.

### Localization Performance

To evaluate the localization performance, we collected two sets of fingerprints at consecutive days (90 locations, 4 orientations each) in our office building keeping the standard WLAN deployment of 4 access points. One fingerprint set was used as a training radio map and the other for localization. As localization algorithm, we use the nearest neighbor in signal space (NNSS) classifier whereby the distance in signal space is computed using the Euclidean distance formula. The reason for choosing this (rather basic) approach is the more direct correspondence between differences in signal space and localization performance. It is noteworthy to mention that other systems like HORUS [25], for example, use more advanced techniques such as a correlation modeler to mitigate the effects of temporal variations in RSSI. However, the model presented in this paper focuses on systematic variations introduced by the trainer’s body.

Using the collected fingerprint data we create three configurations of the training radio map:

- The full (measured) radio map with all orientations
- Four single-orientation radio maps, each with only fingerprints in one orientation for each of the orientations in the set  $\{0^\circ, 90^\circ, 180^\circ, 270^\circ\}$

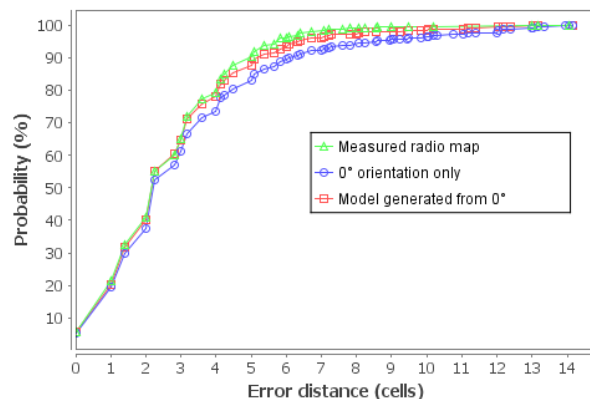


Figure 10. Localization cumulative error distribution

| Orientation        | 0°  | 90° | 180° | 270° |
|--------------------|-----|-----|------|------|
| Single-orientation | 3.2 | 2.9 | 3.1  | 3.0  |
| Model-generated    | 2.8 | 2.7 | 2.8  | 2.9  |

Table 3. Total average error (cells) per orientation

- Four multiple-orientation radio maps generated by applying the model to each of the single-orientation radio maps

We then use the evaluation radio map to perform localization against each of the training radio map configurations. The resulting total average error from the localization across all orientations is shown in Table 3, and Figure 10 shows the cumulative error distribution for the  $0^\circ$  orientation.

The average error obtained when localizing with the full training map is 2.7 cells. We observe (c.f. Table 3) that using only a single orientation results in a performance degradation between 7% and 18%, depending on the chosen orientation. The model-generated radio map consistently outperforms the single-orientation radio map. Compared to the radio map containing all measured orientations, the performance degradation when using the model ranges between 0% and 7%.

In actual localization deployments, the trainer and users of the system are typically not the same person. To evaluate the impact of differences between the trainer and the user, two different persons (70kg and 90kg) collected two sets of fingerprints in the office building (90 locations, 4 orientations

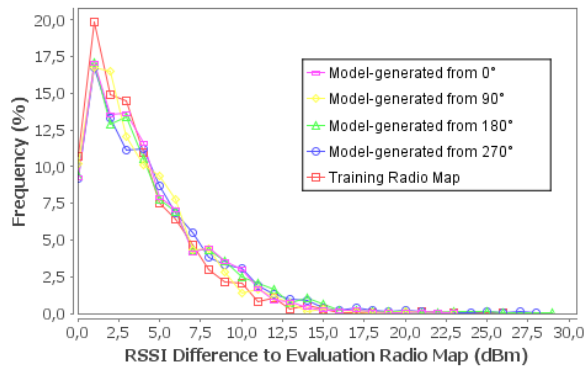


Figure 6. RSSI Deviation for Radio Maps in Library

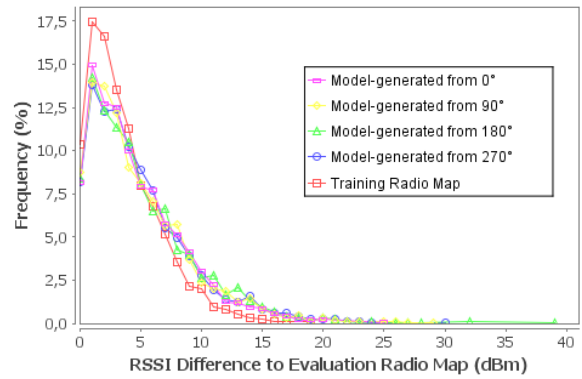


Figure 7. RSSI Deviation for Radio Maps in Home Environment

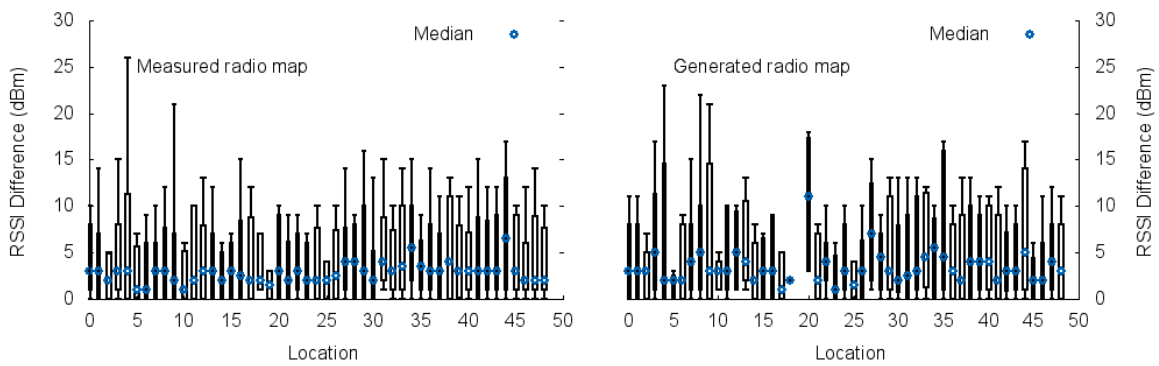


Figure 8. RSSI Deviation per Location in Library

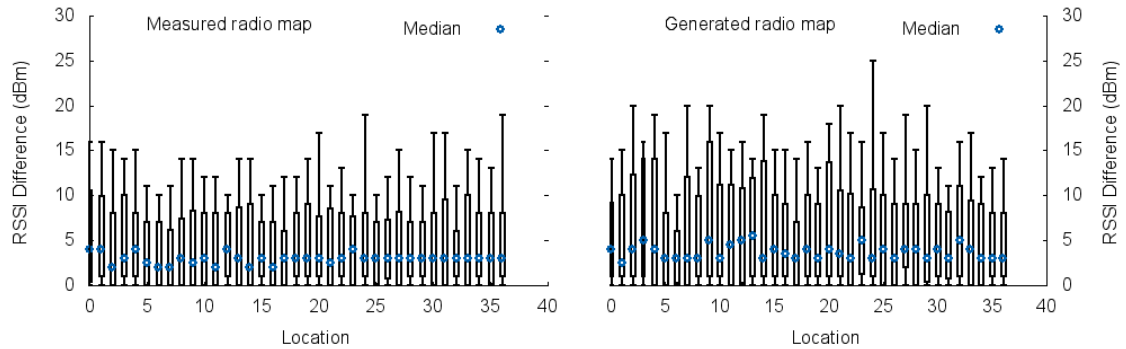


Figure 9. RSSI Deviation per Location for Home Environment

| Orientation        | 0°  | 90° | 180° | 270° |
|--------------------|-----|-----|------|------|
| Single-orientation | 3.0 | 2.8 | 2.9  | 2.9  |
| Model-generated    | 2.7 | 2.7 | 2.7  | 2.7  |

Table 4. Total average error (cells) per orientation (cross-person)

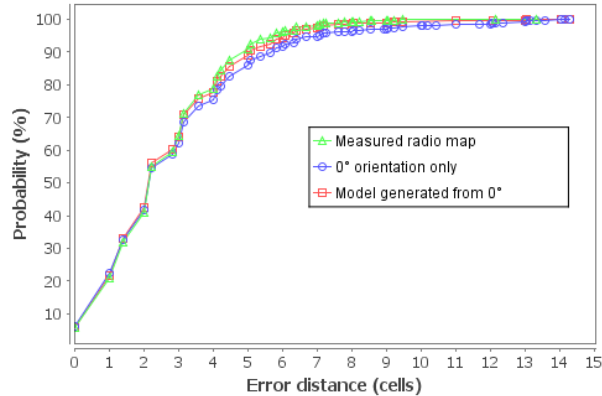


Figure 11. Localization cumulative error distribution with radio maps from different persons

each) on consecutive days. We then used the set of fingerprints collected by the first person for training and the other one for localization. The total average error for the manually measured radio map is 2.7 cells. The total average error for the different single-orientation and generated radio maps is shown in Table 4 and the cumulative error distribution for 0° is shown in Figure 11.

The numbers show a performance improvement of up to 11% when using model-generated radio maps as opposed to single-orientation maps. The performance of model-generated radio map is close to that of the full manually measured radio map. This indicates that the model results in a considerable improvement in localization accuracy even when the trainer and users of the system are different persons.

### Mapping Effort

WLAN signals are typically broadcast over multiple channels and each access point may use any one of the total 14 available channels. The IEEE 802.11 standard requires that all the available channels be scanned in a search for WLAN networks. With most commercial access points having a 100ms beacon interval [24], this means that it typically takes  $100ms * 14 = 1.4s$  to do a complete WLAN scan. Also, due to the typical fluctuations in the WLAN signal measurements even for consecutive measurements at the same position, it is usually recommended to perform more than one WLAN scan to increase the stability of the recorded RSSI value for a given position. In our research, we typically collected 5 duplicate scans for each orientation. With 8 orientations and 90 positions in our office building, the total time required for scanning is  $1.4s * 5 \text{ scans} * 8 \text{ orientations} * 90 \text{ positions} = 5040s$  or 1.4 hours to create a radio map of the building.

If we would instead collect just one fingerprint per orientation and apply the model to generate the other orientations, we would need just 10.5 minutes of pure scanning time. This represents an 87.5% reduction in the effort and even if we

would only collect 4 orientations we would still have a 75% reduction in scanning time. Intuitively, when considering the time required for moving between locations and posturing for multiple orientations, the percentual gains may vary. However, the absolute differences will still be significant, especially, when considering large localization areas.

### CONCLUSION

In this paper, we have presented an approach to modeling signal attenuation caused by the human body during fingerprinting as a means of generating orientation-independent fingerprints for indoor localization. The model is used to enhance WLAN radio maps which contain only fingerprints collected in one orientation into radio maps with fingerprints for multiple orientations. Based on our experimental evaluation, the model generates fingerprints which are comparable to those obtained by manual measurement. In particular, the results indicate the following:

- The generated radio maps are comparable to those obtained by manual measurement of the signal strengths and exhibit consistent minor variations across all locations. Furthermore, the localization performance of the generated radio maps is close to a manually measured one and consistently better than a single-orientation radio map.
- The performance of the signal attenuation model is independent of the orientation used to create the base fingerprint set. It is possible to start with single-orientation fingerprints in any orientation and then reverse generate a multiple-orientation radio map. This makes it easy to apply the model to already deployed localization systems.
- The signal attenuation model is generally applicable and is independent of the physical location, or the person creating the fingerprints. It depends only on the input RSSI which has been manually measured for each location.
- By applying the signal attenuation model, it is possible to save up to 75% to 87.5% WLAN scanning time in the training phase which is a significant gain especially for larger deployments.

In the future we plan to study the effects of environmental changes over longer periods of time with the goal of building a dynamic model which can periodically re-calibrate the radio map.

### ACKNOWLEDGEMENTS

This work is partially supported by UBIQUITEC e.V. (European Center for Ubiquitous Technologies and Smart Cities), GAMBAS (Generic Adaptive Middleware for Behavior-driven Autonomous Services) funded by the European Commission under FP7 with contract FP7-2011-7-287661 and LIVING++ funded by the BMWi under contract number KF2095019FR0.

### REFERENCES

1. P. Bahl and V. Padmanabhan. Radar: an in-building rf-based user location and tracking system. In *INFOCOM 2000*, volume 2, pages 775–784 vol.2. IEEE, 2000.

2. K. Chintalapudi, A. Padmanabha Iyer, and V. N. Padmanabhan. Indoor localization without the pain. *Proc. MobiCom 2010*, page 173, 2010.
3. D. Faria. Modeling signal attenuation in ieee 802.11 wireless lans-vol. 1. *Computer Science Department, Stanford University*, 1, 2005.
4. C. Feng, W. S. A. Au, S. Valaee, and Z. Tan. Orientation-aware indoor localization using affinity propagation and compressive sensing. *CAMSAP 2009*, pages 261–264, 2009.
5. U. Frese. Treemap: An  $o(\log n)$  algorithm for indoor simultaneous localization and mapping. *Autonomous Robots*, 21(2):103–122, 2006.
6. Y. Gu, A. Lo, and I. Niemegeers. A survey of indoor positioning systems for wireless personal networks. *Communications Surveys Tutorials*, 11(1):13–32, 2009.
7. D. Han, D. G. Andersen, M. Kaminsky, K. Papagiannaki, and S. Seshan. Access point localization using local signal strength gradient. In *Proc. PAM 2009*, pages 99–108. Springer-Verlag, 2009.
8. V. Honkavirta, T. Perala, S. Ali-Loytty, and R. Piche. A comparative survey of wlan location fingerprinting methods. In *WPNC 2009*, pages 243–251, 2009.
9. Y. Ji, S. Biaz, S. Pandey, and P. Agrawal. Ariadne: a dynamic indoor signal map construction and localization system. In *Proc. MobiSys 2006*, pages 151–164. ACM, 2006.
10. Y. Jiang, X. Pan, K. Li, Q. Lv, R. P. Dick, M. Hannigan, and L. Shang. Ariel: automatic wi-fi based room fingerprinting for indoor localization. In *Proc. UbiComp 2012*, pages 441–450. ACM, 2012.
11. K. Kaemarungsi. Distribution of wlan received signal strength indication for indoor location determination. In *ISWPC 2006*, pages 1–6. IEEE, 2006.
12. K. Kaemarungsi and P. Krishnamurthy. Modeling of indoor positioning systems based on location fingerprinting. In *INFOCOM 2004*, volume 2, pages 1012–1022. IEEE, 2004.
13. K. Kaemarungsi and P. Krishnamurthy. Properties of indoor received signal strength for WLAN location fingerprinting. *MOBIQUITOUS 2004.*, pages 14–23, 2004.
14. T. King, S. Kopf, T. Haenselmann, C. Lubberger, and W. Effelsberg. Compass: A probabilistic indoor positioning system based on 802.11 and digital compasses. In *Proc. WINTECH 2006*, pages 34–40. ACM, 2006.
15. A. M. Ladd, K. E. Bekris, A. Rudys, G. Marceau, L. E. Kavvaki, and D. S. Wallach. Robotics-based location sensing using wireless ethernet. In *Proc. MobiCom 2002*, pages 227–238. ACM, 2002.
16. H. Lee, H. Kim, and W. Choi. Modeling heterogeneous signal strength characteristics for flexible wlan indoor localization. *ICCAS-SICE 2009*, pages 1765–1768, 2009.
17. M. Lihan, T. Tsuchiya, and K. Koyanagi. Orientation-aware indoor localization path loss prediction model for wireless sensor networks. In *Proc. NBIS 2008*, pages 169–178. Springer-Verlag, 2008.
18. H. Liu, H. Darabi, P. Banerjee, and J. Liu. Survey of wireless indoor positioning techniques and systems. *SMC 2007, Part C: Applications and Reviews*, 37(6):1067–1080, 2007.
19. H. Lukaski. Methods for the assessment of human body composition: traditional and new. *The American journal of clinical nutrition*, 1987.
20. K. Nasr, F. Costen, and S. Barton. Average signal level prediction in an indoor wlan using wall imperfection model. In *PIMRC 2005*, volume 1, pages 674–678. IEEE, 2005.
21. S. Seidel and T. Rappaport. 914 mhz path loss prediction models for indoor wireless communications in multifloored buildings. *APS*, 1992, 40(2):207–217, 1992.
22. S. Sen, R. R. Choudhury, and S. Nelakuditi. Spinloc: Spin once to know your location. *ACM HotMobile*, 2012.
23. A. Varshavsky, D. Pankratov, J. Krumm, and E. D. Lara. Calibree: Calibration-free localization using relative distance estimations. *Pervasive Computing*, pages 146–161, 2008.
24. H. Velayos and G. Karlsson. Techniques to reduce the ieee 802.11b handoff time. In *ICC 2004*, volume 7, pages 3844–3848, 2004.
25. M. Youssef and A. Agrawala. The horus location determination system. *Wireless Networks*, 14(3):357–374, 2008.
26. M. Zhang and S. Zhang. An accurate and fast wlan user location estimation method based on received signal strength. In *Proc. ICCS 2007*, pages 58–65. Springer-Verlag, 2007.